Acta Cryst. (1994). B50, 31–41

Structures of Synthetic $K_2MgSi_5O_{12}$ Leucites by Integrated X-ray Powder Diffraction, Electron Diffraction and ^{29}Si MAS NMR Methods

BY A. M. T. BELL*

Department of Chemistry, Keele University, Keele, Staffordshire ST5 5BG, England

C. M. B. HENDERSON

Department of Geology, University of Manchester, Oxford Road, Manchester M13 9PL, England

S. A. T. REDFERN

Departments of Chemistry and Geology, University of Manchester, Oxford Road, Manchester M13 9PL, England

R. J. CERNIK

SERC Daresbury Laboratory, Warrington WA4 4AD, England

P. E. CHAMPNESS

Department of Geology, University of Manchester, Oxford Road, Manchester M13 9PL, England

A. N. FITCH†

Department of Chemistry, Keele University, Keele, Staffordshire ST5 5BG, England

AND S. C. KOHN

Department of Geology, University of Manchester, Oxford Road, Manchester M13 9PL, England, and Department of Physics, University of Warwick, Coventry CV4 7AL, England

(*Received* 25 *March* 1993; *accepted* 17 *August* 1993)

Abstract

The structures of disordered and ordered varieties of the title compound have been determined using integrated TEM, MAS NMR and Rietveld analysis of synchrotron X-ray powder diffraction data. Both samples have a 'leucite-like' framework topology. The dry-synthesized sample is cubic, $Ia3d$ [a = 13.4190 (1) Å, V = 2416.33 (5) Å^3] with disordered Mg and Si in tetrahedral framework sites. The hydrothermally synthesized analogue is monoclinic, $P2_1/c$ [a = 13.168 (5), b = 13.652 (1), c = 13.072 (5) Å, β = 91.69°, V = 2348 (2) Å^3], and has a fully ordered framework with four K, ten Si and two Mg sites per 24 O atoms (one quarter of the unit cell). Two of these Si sites are linked to Si tetrahedra only [Q^4(4Si)], while the other eight Si sites have one Mg and three Si tetrahedra as next-nearest neighbours [Q^4(3Si,1Mg)]. Q^4(4Si) and Mg tetrahedra share opposite corners of four rings. Si and Mg ordering is accompanied by a volume contraction of 2.8%. The X-ray structural data for the ordered sample allow the ^{29}Si MAS NMR peaks to be assigned to particular Si tetrahedra, and thus to particular values of the mean T—O—T angle. The nature of the polymorphism between the disordered and ordered samples is discussed and related to the different synthesis conditions. Water in the hydrothermal synthesis accelerates Si–Mg ordering, allowing the thermodynamically more stable phase to be formed.

Introduction

The natural mineral leucite ($KAlSi_2O_6$) has a three-dimensional framework of linked silicate and aluminate tetrahedra with channels occupied by potassium ions. Leucite (*sensu stricta*) can be considered to be the 'type structure' of a large family of related compounds, which include both natural and synthetic varieties, and this structure type has consistently attracted the attention of crystallographers

* Present address: SERC Daresbury Laboratory, Warrington WA4 4AD, England.

† Present address: European Synchrotron Radiation Facility, BP 220, F-38043, Grenoble CEDEX, France.

ISSN 0108-7681

since its first description (*e.g.* Wyart, 1940; Faust, 1963; Peacor, 1968; Mazzi, Galli & Gottardi, 1976; Galli, Gottardi & Mazzi, 1978; Murdoch, Stebbins, Carmichael & Pines, 1988; Palmer, Bismayer & Salje, 1990). At elevated temperatures, the leucite structure displays structural phase transitions related to displacive instabilities and the ordering of tetrahedral cations (Al and Si in the type material); these phenomena are of significance to our understanding of the stability relations of leucite in rocks. In addition, possible fast-ion conduction of the large channel cations (K in leucite *s.s.*) indicates that the structural family might be of some technological significance.

The high-temperature, tetragonal–cubic phase transition in natural leucite, first observed by Klein (1884), is of particular interest and is responsible for drastic changes in the physical and chemical properties. This transition can be simply regarded as a displacive collapse of the tetrahedral framework about the large K cation (Taylor & Henderson, 1968). However, the precise effect of Al,Si ordering on this transition and the sub-solidus phase relations of leucite polymorphs still pose intriguing problems. While it is now generally held that Al,Si order does not play a dominant role in this displacive transition (Dove, Cool, Palmer, Putnis, Salje & Winkler, 1993), neutron and X-ray diffraction studies have revealed that the high-temperature polymorph of natural leucite, while metrically cubic, does not display a completely random Al,Si distribution on the tetrahedral (*T*) sites, as demanded by its 'supposed' *Ia3d* space group (*e.g.* Boysen, 1990; Ito, Kuehner & Ghose, 1991). This has led to speculation regarding the thermodynamic nature of such a 'cubic' structure and fuelled discussion regarding the nature of Al,Si ordering on the *T* sites in the framework.

As part of a wider attempt to understand the controls and consequences of tetrahedral-cation ordering in leucites, we are studying a series of 'leucite' analogues of the general formula X_2^+-$Y^{2+}Si_5O_{12}$, related to leucite (*s.s.*) by the coupled framework cation substitution 2Al = Y,Si (Torres-Martinez & West, 1989). Such compounds are more amenable to *T*-site analysis than Al–Si analogues and also display a significant response to *T*-site ordering. For example, Torres-Matinez & West (1986) have shown that dry-synthesized $Rb_2MgSi_5O_{12}$ is cubic *Ia3d* with disordered *T* sites, whereas Heinrich & Baerlocher (1991) found that hydrothermally annealed $Cs_2CuSi_5O_{12}$ is tetragonal $P4_12_12$ with fully ordered *T* sites (six occupied by Si and one by Cu). In the present paper, we will focus on synthetic samples of stoichiometry $K_2MgSi_5O_{12}$. In a MAS NMR study, Kohn, Dupree, Mortuza & Henderson (1991) have shown that dry-synthesized $K_2MgSi_5O_{12}$ leucite shows a disordered arrangement of *T* cations, while hydrothermally synthesized samples have an ordered arrangement of Si and Mg on tetrahedral sites. The full interpretation and further understanding of these relations has, so far, been limited by a lack of structural data, mainly because samples are only available as fine-grained powders. Here, therefore, we report the results of Rietveld refinements (Rietveld, 1969) of synchrotron X-ray data from these two types of $K_2MgSi_5O_{12}$ and describe their structures.

Experimental methods and results

Sample preparation

Dried, high-purity K_2CO_3, MgO and SiO_2 were weighed to give a stoichiometry equivalent to $K_2MgSi_5O_{12}$, thoroughly mixed, pre-heated to 873 K to decompose the carbonate, and melted at 1523 K for 24 h in a platinum crucible. The crucible and contents were then quenched in liquid nitrogen. The resultant glass was analysed by electron microprobe and found to be homogeneous and stoichiometric. A sample of powdered glass was then heated at 1073 K for 5 d in air to produce a crystalline powder, hereafter described as the dry-synthesized sample. A second portion of the starting material was annealed at a temperature of 873 K and a water-vapour pressure of 0.5×10^8 Pa for 7 d in a hydrothermal 'cold-seal' pressure vessel.

Initial X-ray characterization

Powder patterns were obtained with a laboratory X-ray diffractometer (Philips PW 1050), using Cu $K\alpha$ radiation. Kohn *et al.* (1991) summarized the features of the powder patterns obtained for the two samples and pointed out that the dry-synthesized sample is cubic [cell parameter a = 13.419 (6) Å, V = 2416 Å^3], space group *Ia3d*. By contrast, the hydrothermal sample shows overall features similar to those of a tetragonal-leucite powder pattern but with many split peaks. Pseudo-orthorhombic cell parameters were given as a = 13.13 (4), b = 13.04 (4), c = 13.64 (4) Å, V = 2335 Å^3.

^{29}Si *MAS NMR*

The NMR spectra described here were obtained using a Bruker MSL 360 spectrometer (8.45 T) operating at 71.5 MHz. Kohn *et al.* (1991) have already presented the results for both the dry- and hydrothermally synthesized samples but the main features will be summarized here. The ^{29}Si NMR spectrum of the dry-crystallized $K_2MgSi_5O_{12}$ sample consists of a rather broad peak [FWHM = 13 p.p.m., *cf.* 17 p.p.m. for the glass starting material (Fig. 1)],

indicating a wide distribution of Si environments. The centres of gravity of the resonances of the dry-crystallized and the glassy samples are very similar; the small change from −95.7 p.p.m. for the glass to −94.8 p.p.m. for the crystalline sample could suggest that the mean Si—O—*T* angles are smaller in the latter. Although the Si environment in the dry-synthesized sample is very variable on this local scale, on the longer length scale probed by X-ray diffraction, the averaged environment results in the single *T* site required by the space-group symmetry *Ia3d*. The ^{29}Si spectrum for the hydrothermal sample shows ten sharp peaks of approximately equal intensity with chemical shifts in the range −84.6 to −104.5 p.p.m. (Fig. 1), consistent with the presence of ten distinct Si sites in the $K_2MgSi_5O_{12}$ structure. Since there are two Mg atoms for every ten Si atoms, Kohn *et al.* deduced that the structure contains 12 distinct *T* sites and that all the Mg and Si atoms are ordered on these sites. Two of the ^{29}Si lines have small chemical-shift anisotropies characteristic of Si tetrahedra linked to four other Si tetrahedra [Q^4(4Si)]; the other eight Si lines are as a result of Si tetrahedra linked to three SiO_4 tetrahedra and one MgO_4 tetrahedron [Q^4(3Si,1Mg)]. The absence of peaks as a result of Q^4(2Si,2Mg) indicates that the Mg atoms are as far apart as possible. The chemical shifts of some of the Si peaks are consistent with the presence of some very small *T*—O—*T* angles. Two-dimensional ^{29}Si correlation spectroscopy (COSY) experiments enabled the overall topology of the unit cell to be deduced.

Electron diffraction

Using the synchrotron X-ray powder pattern for the hydrothermally synthesized sample, it was not possible initially to determine the cell parameters accurately and to index all of the reflections unambiguously, mainly because the first (very weak) reflection appeared to be missing. The sample was therefore examined by electron diffraction in a transmission electron microscope to see if the space group could be determined.

An ion-thinned grain mount of the sample was mounted in the liquid-nitrogen-cooled double-tilt holder of a Philips EM430 TEM operating at 300 keV. Grains transparent to the electron beam were tilted in reciprocal space in both directions about their shortest reciprocal lattice direction. Each major zone thus encountered was recorded photographically and the tilt angles noted. All the patterns could be indexed using the pseudo-orthorhombic cell parameters derived by X-ray diffraction; however, in the results presented below, the *b* and *c* axes have been transposed, namely $a = 13.13$, $b = 13.64$ and $c = 13.04$ Å.

The lack of systematic absences in *hkl* reflections indicates that the lattice is primitive. The [010] pattern (Fig. 2*a*) shows that $\beta^* = 92°$ and that the reflections $l \neq 2n$ are extremely weak in the zero-order Laue zone (ZOLZ), but strong in the

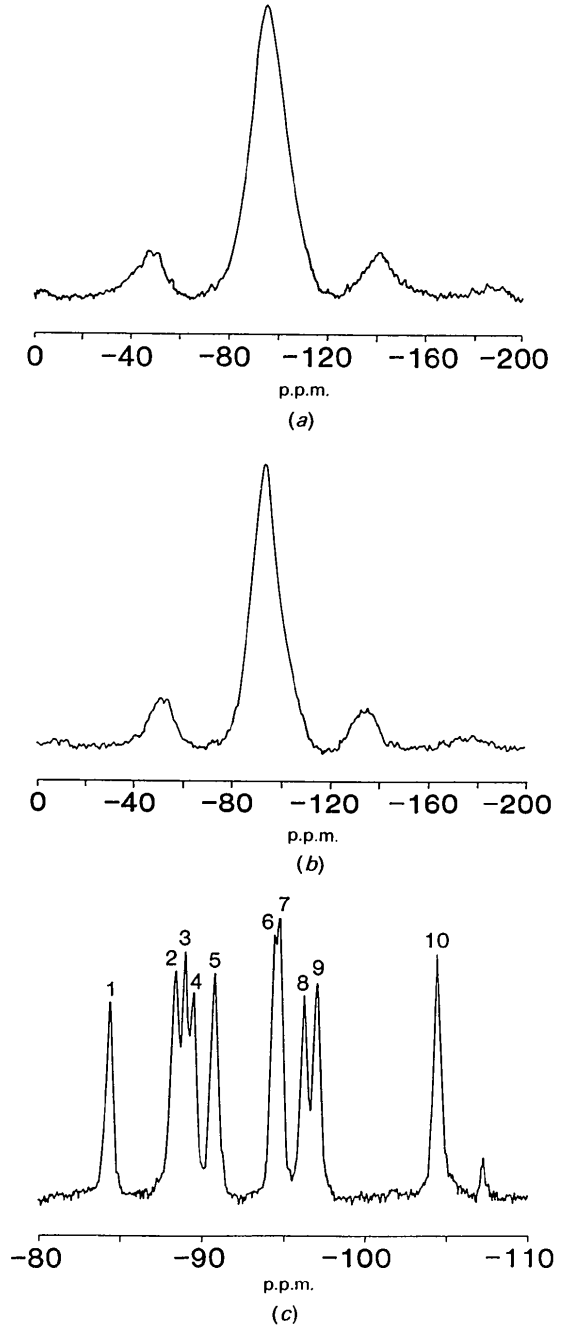

Fig. 1. ^{29}Si MAS NMR spectra of $K_2MgSi_5O_{12}$ 'leucites': (*a*) glass starting material; (*b*) dry-synthesized; (*c*) hydrothermally synthesized. (*b*) and (*c*) after Kohn *et al.* (1991). The small peak at −107 p.p.m. in (*c*) is as a result of a quartz impurity (about 2%).

higher-order Laue zones (HOLZ's). This suggests the presence of a *c*-glide plane parallel to (010). The [100] pattern (Fig. 2*b*) appears to show no systematic absences and has $\alpha^* = 90°$. However, when the specimen is tilted about b^* from the [100] zone, the $k \neq 2n$ reflections become extremely weak compared with the $k = 2n$ reflections. This suggests the presence of a screw diad parallel to y, the strong $k \neq 2n$ reflections which appear at the exact zone axis being derived by double diffraction from within the ZOLZ.

The above data suggest that the structure of the hydrothermally synthesized sample is a distorted, monoclinic version of the cubic structure of the dry-synthesized sample and that the space group is probably $P2_1/c$.

Synchrotron X-ray powder diffraction

The structures of the two synthetic $K_2MgSi_5O_{12}$ leucite samples were then determined using high-resolution synchrotron X-ray powder-diffraction methods. The samples were loaded onto aluminium flat-plate containers, 15 mm in diameter and 1 mm in depth, and data were collected in the ranges 8–100° 2θ (dry sample) and 8–130° 2θ (hydrothermal sample) in 10 millidegree steps on station 8.3 of the SRS at the SERC Daresbury Laboratory (Cernik, Murray, Pattison & Fitch, 1990). The wavelength [$\lambda = 1.52904$ (1) Å] was calibrated using six reflections from a standard Si sample (NBS 640b). The synchrotron powder-diffraction data were analysed using the Powder Diffraction Program Library (PDPL) (Murray, Cockcroft & Fitch, 1990). All the data were normalized to correct for beam decay.

Dry-synthesized sample. The dry-synthesized sample was found to be body-centred cubic, space group *Ia3d*, from the systematic absences in the powder pattern and thus is similar to the metrically cubic, high-temperature polymorph of natural leucite (Peacor, 1968) and to pollucite ($CsAlSi_2O_6$; Beger, 1969). The high-temperature single-crystal structure of leucite was therefore used as a starting point to refine the dry $K_2MgSi_5O_{12}$ structure, with Mg + Si replacing 2Al and assuming that all 48 *T* sites are disordered. These *T* sites are all located on the 48(*g*) Wyckoff special position. The background was fitted by making linear connections between 48 background points (distributed between Bragg reflections over the whole pattern) in the range 8–100° 2θ; 109 Bragg reflections occurred in the scan range. A pseudo-Voigt peak-shape function was used to fit each Bragg reflection to the profile. Because of the inherent covalency of the tetrahedral framework, neutral-atom scattering factors were used throughout and were taken from *International Tables for X-ray Crystallography* (1974, Vol. IV); terms for anomalous dispersion were not included. The atomic coordinates for K, Si + Mg and O were refined, together with lattice parameters, the pseudo-Voigt mixing parameter, zero point and three half-width parameters. The refinement converged to give the structural parameters and *R* factors summarized in Table 1. The agreement between the observed and calculated profiles in the Rietveld difference plot is shown in Fig. 3. Bond lengths and bond angles

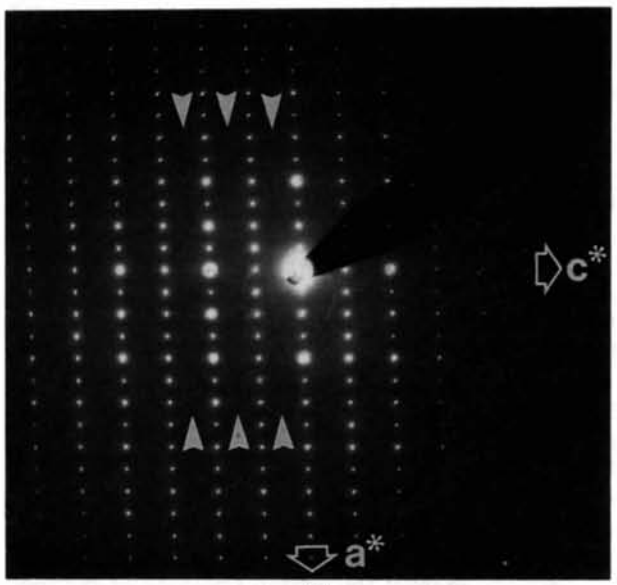

(*a*)

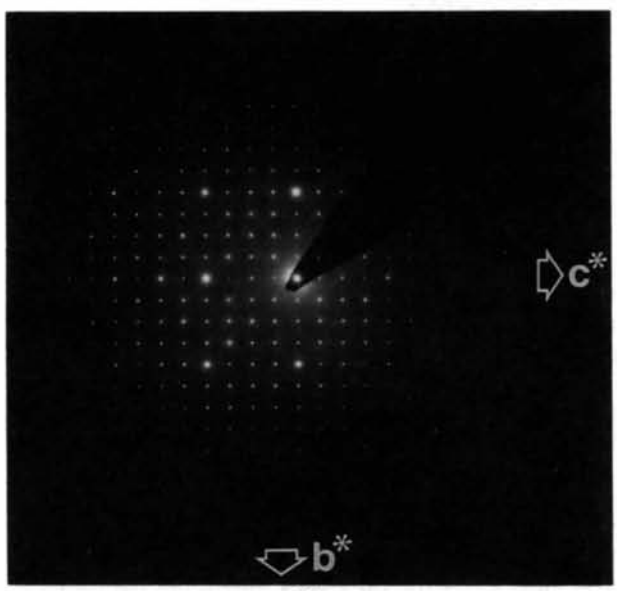

(*b*)

Fig. 2. Electron-diffraction patterns of hydrothermally synthesized $K_2MgSi_5O_{12}$ leucite: (*a*) [010] pattern, note the rows of very weak reflections for *l* odd (arrowed); (*b*) [100] pattern, note that the rows of reflections for which *l* is odd are strong in this pattern.

Table 1. *Refined structural parameters for dry-synthesized* $K_2MgSi_5O_{12}$

Cell parameters: $a = 13.4190$ (1) Å, $V = 2416.33$ (5) Å^3.
The structure was refined with the following R factors: $R_I = 8.81$, $R_{wp} = 13.85$, $R_e = 13.82\%$.
N = number of atoms in the unit cell.

		x	y	z	B_{iso}	N
K	16(b)	0.125	0.125	0.125	12.8 (1)	16.0
Si	48(g)	0.125	0.6616 (2)	0.5884 (2)	5.42 (7)	40.0
Mg	48(g)	0.125	0.6616 (2)	0.5884 (2)	5.42 (7)	8.0
O	96(h)	0.4684 (3)	0.3847 (2)	0.1446 (2)	10.0 (1)	96.0

Table 2. *Bond lengths* (Å) *and angles* (°) *for dry-synthesized* $K_2MgSi_5O_{12}$

T—O	1.589 (4)
T—O	1.631 (3)
O—T—O(×2)	112.5 (2)
O—T—O(×2)	110.5 (2)
O—T—O	104.6 (2)
O—T—O	106.4 (2)
Mean	109.5 ($\sigma^2 = 10.7$)*
K—O(×6)	3.470 (3)
K—O(×6)	3.339 (3)
T—O—T	144.5 (2)

* Tetrahedral angle variance: $\sigma^2 = \Sigma(\theta - 109.47)^2/5$.

calculated from the atomic coordinates are given in Table 2 and the refined structure is illustrated in Fig. 4.

The T—O bond length is only slightly larger than that for tetrahedrally coordinated Si—O in framework silicates (1.59–1.63 Å; *International Tables for X-ray Crystallography*, 1985, Vol. III). The two sets of six K—O distances for the W site, located within the open ⟨111⟩ channels, have distinctly different values (3.34 and 3.47 Å) which are similar to those found for high-temperature $KAlSi_2O_6$ leucite (3.37 and 3.57 Å; Peacor, 1968), for Rb—O in $Rb_2MgSi_5O_{12}$ (3.29 and 3.60 Å; Torres-Martinez & West, 1986) and Cs—O in pollucite (3.39 and 3.56 Å; Beger, 1969). The isotropic temperature factors (Table 1) are uniformly high for all atom types. The individual O—T—O angles show a considerable range with a tetrahedral angle variance (σ^2; Robinson, Gibbs & Ribbe, 1971) of 10.7 deg^2 (Table 2).

Hydrothermally synthesized sample. The superimposed diffraction patterns of the dry- and hydrothermally synthesized samples are shown in Fig. 5. Clear similarities are apparent between the two patterns as groups of Bragg reflections in the hydrothermal sample coincide with individual reflections in the dry, cubic sample. These similarities are consistent with both samples having the same framework topology. In addition, the closely similar cell volumes suggest that both unit cells have the same contents.

The starting model for the structure determination of the hydrothermal material therefore was based on the cubic coordinates determined for the dry-synthesized sample, transferred to the monoclinic cell determined by electron diffraction. It was found that the cubic coordinates could all be related by the symmetry operations for $P2_1/c$, which was therefore adopted as the correct space group for the hydrothermal sample. In the $P2_1/c$ cell, all atoms are located on general positions. To accommodate 48 T atoms, 12 different 4(e) positions are required which confirms the deduction from the NMR results of 12 T sites (10Si and 2Mg; Kohn *et al.*, 1991).

The same Rietveld refinement procedure as for the dry-synthesized material was used, with the excep-

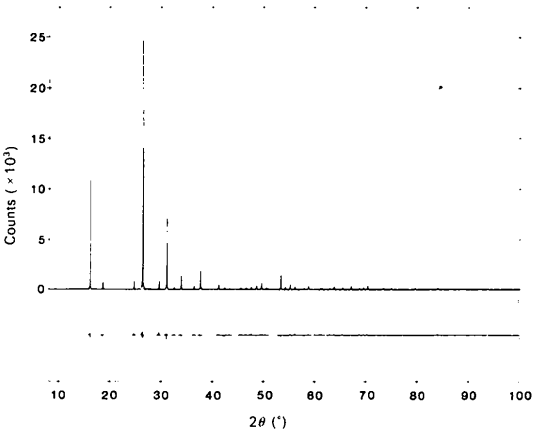

Fig. 3. Rietveld difference plot for dry-synthesized $K_2MgSi_5O_{12}$ leucite.

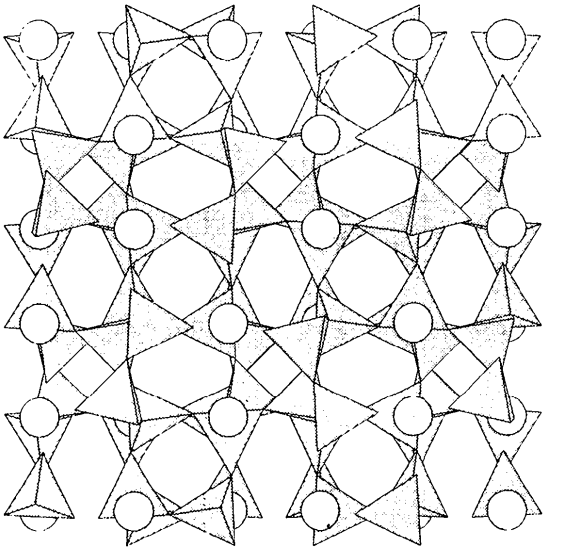

Fig. 4. Cubic structure of dry-synthesized $K_2MgSi_5O_{12}$ leucite; projection (100).

tion that the background was subtracted by making linear connections between 17 background points and then fitting a second-order polynomial to this background. There were 1062 Bragg reflections in the data set in the range 8–70° 2θ; the data between 70 and 130° 2θ were excluded as the signal/noise ratio was very poor in this region. Some weak reflections that could not be assigned to the monoclinic leucite phase were found to be as a result of a small amount of quartz impurity; this confirms the NMR identification (Kohn *et al.*, 1991). The final unit-cell parameters from the Rietveld refinement are: a = 13.168 (5), b = 13.652 (1), c = 13.072 (5) Å, β = 91.69 (5)°. [Note that the e.s.d. for b reported by the program is anomalously low (0.0001 Å) and we have chosen to assign a more reasonable value of 0.001 Å.]

In the first stage of the refinement, all the T—O distances were constrained to a value of 1.63 (2) Å, the upper value determined for the dry sample. The scattering factor for the neutral Si atom was used for all 12 T sites. Once an initial fit was obtained, peaks from the quartz impurity were included in a two-phase Rietveld analysis. The K- and T-atom coordinates were then refined and observed to move away from the special positions of the cubic space group. The O-atom coordinates were then refined, after which it was apparent that two of the T sites (sites 5 and 6) exhibited mean T—O distances >1.73 Å, whereas those for the other ten sites ranged from 1.61 to 1.68 Å. The refinement procedure was then changed so that the T—O distances in each tetrahedral unit were constrained, but the mean T—O distances for each unit were allowed to differ. During further refinement, the two 'long' T—O mean distances for sites 5 and 6 increased to 1.9 and 1.86 Å and the other ten distances remained in the range 1.59–1.64 Å. The two sites with the long mean T—O distances are clearly those occupied by Mg (*cf.* tetrahedral Mg—O distance of 1.915 Å in akermanite; Kimata & Ii, 1981). The scattering factor for neutral Mg was therefore substituted for the Si scattering factor for sites 5 and 6 and the structural refinement was completed.

The observed and calculated profiles in the Rietveld difference plot show a good match, indicating that the determined structure is reliable (Fig. 6). The final refined structural parameters and R factors are given in Table 3 and the calculated bond lengths and angles in Tables 4, 5, 6 and 7.* The mean Si—O and Mg—O bond lengths are typical of tetrahedral coordination in framework structures. The four cavity-cation sites ('W sites') all show highly distorted K—O polyhedra with 12 K—O bond lengths varying from 2.64 to 3.97 Å, indicating an exceptionally large coordination polyhedron. The mean K—O distances for K1 and K2 (Table 6) are distinctly longer than those for K3 and K4. Individual O—T—O bond angles for both Si and Mg T sites show significantly different distortions. Si—O—Si inter-tetrahedral bond angles vary from 130 to 160° (mean 141°) while Si—O—Mg angles are significantly smaller, in the range 119.8–147° (mean 130.6°) (Table 7). The tetrahedral-angle variance (σ^2) for Si sites averages 20.9 (9.9) deg^2 while that for Mg sites is somewhat higher at 40.4 (8.8) deg^2 (Table 3). Temperature factors for the different elements (Table 3) are much smaller than those found for the dry-synthesized sample (Table 1).

From the connectivity information given in Table 7, it can be seen that Si sites 9 and 12 are only linked to their next-nearest neighbour (NNN) Si atoms.

* Copies of the powder diffraction data have been deposited with the British Library Document Supply Centre as Supplementary Publication No. SUP 71349 (35 pp.). Copies may be obtained through The Technical Editor, International Union of Crystallography, 5 Abbey Square, Chester CH1 2HU, England. [CIF reference: LI0152]

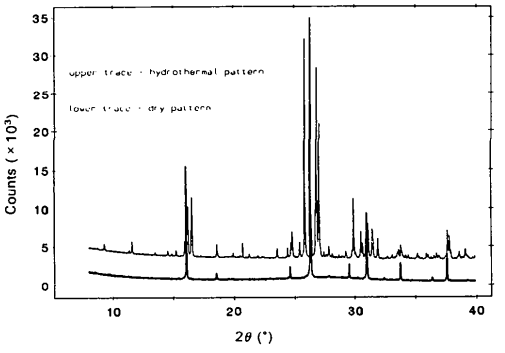

Fig. 5. Superimposed X-ray diffraction traces for dry- and hydrothermally synthesized $K_2MgSi_5O_{12}$ leucites. Note that single peaks in the cubic material are split into several individuals in the monoclinic form.

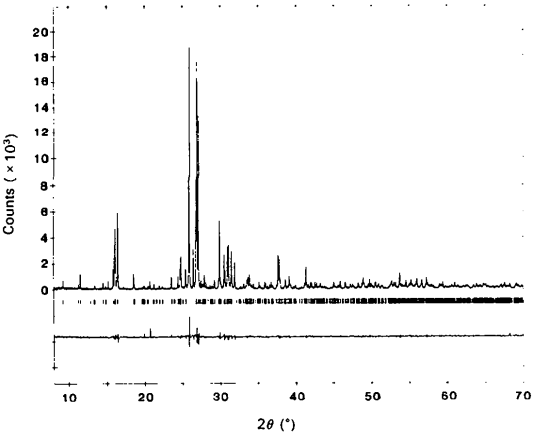

Fig. 6. Rietveld difference plot for hydrothermally synthesized $K_2MgSi_5O_{12}$ leucite.

Table 3. *Refined structural parameters for hydrothermal* $K_2MgSi_5O_{12}$

Cell parameters: $a = 13.168$ (5), $b = 13.652$ (1), $c = 13.072$ (5) Å, $\beta = 91.69$ (5)°, $V = 2348$ (2) Å^3.
The structure was refined with the following R factors: $R_I = 4.67$, $R_{wp} = 11.58$, $R_e = 7.07\%$.

		x	*y*	*z*	B_{iso}	*N*
K1	4(*e*)	0.1138 (6)	0.1103 (6)	0.0948 (5)	3.3 (1)	4.0
K2	4(*e*)	0.6289 (5)	0.3956 (6)	0.8522 (5)	3.3 (1)	4.0
K3	4(*e*)	0.3681 (6)	0.3597 (6)	0.3747 (5)	3.3 (1)	4.0
K4	4(*e*)	0.8534 (6)	0.1322 (6)	0.6461 (5)	3.3 (1)	4.0
Si1	4(*e*)	0.1081 (7)	0.6789 (6)	0.5689 (6)	0.48 (8)	4.0
Si2	4(*e*)	0.6433 (7)	0.8186 (6)	0.4014 (7)	0.48 (8)	4.0
Si3	4(*e*)	0.5776 (7)	0.1445 (6)	0.6328 (6)	0.48 (8)	4.0
Si4	4(*e*)	0.0948 (7)	0.3507 (6)	0.3128 (6)	0.48 (8)	4.0
Mg5	4(*e*)	0.6420 (7)	0.5710 (6)	0.1089 (7)	0.3 (2)	4.0
Mg6	4(*e*)	0.1865 (7)	0.9352 (6)	0.8683 (7)	0.3 (2)	4.0
Si7	4(*e*)	0.4082 (7)	0.8613 (6)	0.9526 (6)	0.48 (8)	4.0
Si8	4(*e*)	0.8988 (7)	0.3880 (7)	0.8670 (6)	0.48 (8)	4.0
Si9	4(*e*)	0.8529 (7)	0.9038 (7)	0.4047 (6)	0.48 (8)	4.0
Si10	4(*e*)	0.8727 (6)	0.6382 (6)	0.1251 (6)	0.48 (8)	4.0
Si11	4(*e*)	0.3911 (6)	0.1119 (7)	0.1620 (7)	0.48 (8)	4.0
Si12	4(*e*)	0.3225 (7)	0.5984 (7)	0.6491 (6)	0.48 (8)	4.0
O1	4(*e*)	0.4576 (9)	0.350 (1)	0.163 (1)	0.2 (1)	4.0
O2	4(*e*)	0.979 (1)	0.162 (1)	0.845 (1)	0.2 (1)	4.0
O3	4(*e*)	0.159 (1)	0.4294 (8)	0.378 (1)	0.2 (1)	4.0
O4	4(*e*)	0.603 (1)	0.0553 (9)	0.555 (1)	0.2 (1)	4.0
O5	4(*e*)	0.370 (1)	0.1846 (9)	0.4772 (9)	0.2 (1)	4.0
O6	4(*e*)	0.905 (1)	0.372 (1)	0.5432 (9)	0.2 (1)	4.0
O7	4(*e*)	0.6719 (9)	0.429 (1)	0.607 (1)	0.2 (1)	4.0
O8	4(*e*)	0.676 (1)	0.7109 (8)	0.364 (1)	0.2 (1)	4.0
O9	4(*e*)	0.357 (1)	0.635 (1)	0.7602 (8)	0.2 (1)	4.0
O10	4(*e*)	0.2174 (9)	0.059 (1)	0.349 (1)	0.2 (1)	4.0
O11	4(*e*)	0.115 (1)	0.7979 (8)	0.556 (1)	0.2 (1)	4.0
O12	4(*e*)	0.918 (1)	0.868 (1)	0.3076 (8)	0.2 (1)	4.0
O13	4(*e*)	0.9854 (8)	0.900 (1)	0.667 (1)	0.2 (1)	4.0
O14	4(*e*)	0.5230 (9)	0.612 (1)	0.427 (1)	0.2 (1)	4.0
O15	4(*e*)	0.683 (1)	0.9813 (8)	0.863 (1)	0.2 (1)	4.0
O16	4(*e*)	0.126 (1)	0.5172 (8)	0.067 (1)	0.2 (1)	4.0
O17	4(*e*)	0.874 (1)	0.665 (1)	0.0023 (8)	0.2 (1)	4.0
O18	4(*e*)	0.405 (1)	0.857 (1)	0.0744 (8)	0.2 (1)	4.0
O19	4(*e*)	0.2125 (8)	0.856 (1)	0.129 (1)	0.2 (1)	4.0
O20	4(*e*)	0.148 (1)	0.2539 (7)	0.823 (1)	0.2 (1)	4.0
O21	4(*e*)	0.833 (1)	0.115 (1)	0.2631 (9)	0.2 (1)	4.0
O22	4(*e*)	0.7359 (9)	0.612 (1)	0.867 (1)	0.2 (1)	4.0
O23	4(*e*)	0.609 (1)	0.2487 (8)	0.086 (1)	0.2 (1)	4.0
O24	4(*e*)	0.441 (1)	0.395 (1)	0.7773 (9)	0.2 (1)	4.0

Table 4. *T*—O *bond lengths* (Å) *for hydrothermal* $K_2MgSi_5O_{12}$

Si(1)—O(2)	1.64 (2)	Si(7)—O(7)	1.59 (2)
Si(1)—O(6)	1.63 (1)	Si(7)—O(14)	1.60 (1)
Si(1)—O(11)	1.64 (1)	Si(7)—O(18)	1.60 (1)
Si(1)—O(19)	1.63 (1)	Si(7)—O(23)	1.60 (1)
Mean	1.63		1.60
Si(2)—O(1)	1.61 (1)	Si(8)—O(11)	1.60 (1)
Si(2)—O(5)	1.60 (1)	Si(8)—O(13)	1.61 (1)
Si(2)—O(8)	1.61 (1)	Si(8)—O(16)	1.60 (2)
Si(2)—O(22)	1.62 (2)	Si(8)—O(21)	1.59 (1)
Mean	1.61		1.60
Si(3)—O(1)	1.64 (1)	Si(9)—O(12)	1.63 (2)
Si(3)—O(4)	1.63 (1)	Si(9)—O(16)	1.62 (1)
Si(3)—O(9)	1.63 (1)	Si(9)—O(17)	1.60 (1)
Si(3)—O(23)	1.64 (1)	Si(9)—O(22)	1.62 (1)
Mean	1.63		1.61
Si(4)—O(2)	1.61 (2)	Si(10)—O(10)	1.64 (2)
Si(4)—O(3)	1.60 (2)	Si(10)—O(13)	1.65 (1)
Si(4)—O(12)	1.60 (1)	Si(10)—O(17)	1.65 (1)
Si(4)—O(20)	1.59 (1)	Si(10)—O(20)	1.65 (1)
Mean	1.60		1.65
Mg(5)—O(4)	1.93 (1)	Si(11)—O(8)	1.64 (2)
Mg(5)—O(5)	1.92 (1)	Si(11)—O(14)	1.65 (2)
Mg(5)—O(10)	1.92 (2)	Si(11)—O(15)	1.63 (2)
Mg(5)—O(24)	1.93 (2)	Si(11)—O(24)	1.63 (1)
Mean	1.92		1.64
Mg(6)—O(3)	1.89 (1)	Si(12)—O(9)	1.59 (1)
Mg(6)—O(6)	1.90 (2)	Si(12)—O(15)	1.61 (1)
Mg(6)—O(7)	1.88 (1)	Si(12)—O(18)	1.60 (1)
Mg(6)—O(21)	1.86 (2)	Si(12)—O(19)	1.59 (1)
Mean	1.88		1.60

Overall: Mean Si—O 1.62 (2)
Mean Mg—O 1.90 (3)

Thus, *T* sites 9 and 12 are the Q^4(4Si) sites (NMR notation); all other Si sites are linked to one Mg NNN atom [*i.e.* Q^4(3Si,1Mg)]. The structure of the fully ordered, hydrothermally crystallized sample is shown in Fig. 7 with the three different *T*-site species identified with different shadings.

Discussion

Temperature factors

The dry-synthesized $K_2MgSi_5O_{12}$ leucite has isotropic temperature factors about twice those for equivalent atoms in *Ia3d* $Rb_2MgSi_5O_{12}$ leucite (Torres-Martinez & West, 1986). Both materials have disordered O positions associated with the random arrangement of Si—O and Mg—O tetrahedra. Thus, in addition to inherent static disorder, the particularly large vibrations possible for the smaller and lighter cavity cation (*i.e.* K) in the large *W* sites must be crucial.

The smaller temperature factors for Si, Mg and O in hydrothermally synthesized relative to dry-synthesized $K_2MgSi_5O_{12}$ leucite results from the ordering of Si and Mg in the framework in the former sample. The fact that the temperature factors for O atoms in the ordered structure are smaller than those for the framework cations is likely to be the result of using neutral scattering factors. Charged scattering factors might 'balance' the temperature factors, but would not significantly affect the structural model.

The very large temperature factor determined for K in the dry-synthesized sample is very similar to that observed in the high-temperature 'cubic' phase of $KAlSi_2O_6$ leucite (Peacor, 1968). In the latter case, the large temperature factor has been associated with enhanced mobility of K^+ at high temperature, to the extent that such leucites display fast-ion conduction associated with site hopping in the channels (Palmer & Salje, 1990). While such high-temperature behaviour might not be responsible for the large isothermal temperature factor observed here for cubic $K_2MgSi_5O_{12}$ leucite, it does illustrate the weakness of the relatively ionic K—O bond. Furthermore, the refinement of the monoclinic-ordered structure shows four sites for K and spatial disorder of the K-site positions within the cubic polymorph is

Table 5. O—*T*—O *bond angles* (°) *for hydrothermal* $K_2MgSi_5O_{12}$

O(2)—Si(1)—O(6)	119.7 (8)	O(7)—Si(7)—O(14)	112.5 (8)
O(2)—Si(1)—O(11)	104.8 (9)	O(7)—Si(7)—O(18)	118.2 (9)
O(2)—Si(1)—O(19)	103.0 (8)	O(7)—Si(7)—O(23)	107.5 (8)
O(6)—Si(1)—O(11)	109.9 (8)	O(14)—Si(7)—O(18)	105.6 (8)
O(6)—Si(1)—O(19)	111.9 (8)	O(14)—Si(7)—O(23)	106.1 (9)
O(11)—Si(1)—O(19)	106.6 (7)	O(18)—Si(7)—O(23)	106.2 (9)
Mean	109.3 (36.5)*	Mean	109.4 (25.3)
O(1)—Si(2)—O(5)	114.3 (9)	O(11)—Si(8)—O(13)	112.4 (7)
O(1)—Si(2)—O(8)	108.0 (9)	O(11)—Si(8)—O(16)	104.6 (8)
O(1)—Si(2)—O(22)	108.2 (8)	O(11)—Si(8)—O(21)	116.4 (8)
O(5)—Si(2)—O(8)	108.5 (8)	O(13)—Si(8)—O(16)	106.0 (9)
O(5)—Si(2)—O(22)	113.5 (8)	O(13)—Si(8)—O(21)	105.3 (8)
O(8)—Si(2)—O(22)	103.7 (7)	O(16)—Si(8)—O(21)	111.9 (8)
Mean	109.4 (15.5)	Mean	109.4 (23.13)
O(1)—Si(3)—O(4)	113.8 (9)	O(12)—Si(9)—O(16)	112.2 (9)
O(1)—Si(3)—O(9)	106.4 (8)	O(12)—Si(9)—O(17)	111.3 (9)
O(1)—Si(3)—O(23)	107.9 (9)	O(12)—Si(9)—O(22)	103.8 (7)
O(4)—Si(3)—O(9)	111.2 (8)	O(16)—Si(9)—O(17)	110.5 (8)
O(4)—Si(3)—O(23)	111.9 (8)	O(16)—Si(9)—O(22)	110.9 (7)
O(9)—Si(3)—O(23)	105.1 (8)	O(17)—Si(9)—O(22)	108.0 (7)
Mean	109.4 (11.7)	Mean	109.4 (9.64)
O(2)—Si(4)—O(3)	115.2 (9)	O(10)—Si(10)—O(13)	111.8 (8)
O(2)—Si(4)—O(12)	101.9 (8)	O(10)—Si(10)—O(17)	111.8 (9)
O(2)—Si(4)—O(20)	107.7 (9)	O(10)—Si(10)—O(20)	111.7 (8)
O(3)—Si(4)—O(12)	117.6 (9)	O(13)—Si(10)—O(17)	110.7 (9)
O(3)—Si(4)—O(20)	109.4 (8)	O(13)—Si(10)—O(20)	107.9 (9)
O(12)—Si(4)—O(20)	104.2 (9)	O(17)—Si(10)—O(20)	102.5 (8)
Mean	109.3 (37.4)	Mean	109.2 (13.68)
O(4)—Mg(5)—O(5)	119.4 (7)	O(8)—Si(11)—O(14)	103.5 (8)
O(4)—Mg(5)—O(10)	105.7 (6)	O(8)—Si(11)—O(15)	106.5 (7)
O(4)—Mg(5)—O(24)	110.7 (7)	O(8)—Si(11)—O(24)	115.6 (9)
O(5)—Mg(5)—O(10)	107.3 (6)	O(14)—Si(11)—O(15)	105.9 (9)
O(5)—Mg(5)—O(24)	102.5 (6)	O(14)—Si(11)—O(24)	113.0 (8)
O(10)—Mg(5)—O(24)	111.2 (7)	O(15)—Si(11)—O(24)	111.5 (9)
Mean	109.5 (34.1)	Mean	109.2 (22.27)
O(3)—Mg(6)—O(6)	106.1 (7)	O(9)—Si(12)—O(15)	114.5 (9)
O(3)—Mg(6)—O(7)	102.9 (6)	O(9)—Si(12)—O(18)	105.0 (7)
O(3)—Mg(6)—O(21)	113.7 (8)	O(9)—Si(12)—O(19)	105.3 (8)
O(6)—Mg(6)—O(7)	121.1 (7)	O(15)—Si(12)—O(18)	110.1 (8)
O(6)—Mg(6)—O(21)	108.7 (7)	O(15)—Si(12)—O(19)	109.6 (7)
O(7)—Mg(6)—O(21)	104.5 (8)	O(18)—Si(12)—O(19)	112.3 (8)
Mean	109.5 (46.6)	Mean	109.5 (14.22)

Mean (σ^2) for SiO_4 = 20.9 (9.9)
Mean (σ^2) for MgO_4 = 40.4 (8.8)

* Tetrahedral-angle variance (σ^2).

Table 6. K—O *bond lengths* (Å) *for hydrothermal* $K_2MgSi_5O_{12}$

K(1)—O(2)	3.73 (1)	K(3)—O(1)	3.04 (1)
K(1)—O(3)	2.97 (1)	K(3)—O(3)	2.91 (2)
K(1)—O(6)	3.72 (2)	K(3)—O(5)	2.74 (1)
K(1)—O(6)	2.82 (2)	K(3)—O(7)	2.95 (2)
K(1)—O(8)	3.12 (2)	K(3)—O(8)	3.75 (2)
K(1)—O(10)	3.63 (2)	K(3)—O(8)	3.62 (2)
K(1)—O(12)	3.77 (2)	K(3)—O(14)	2.95 (1)
K(1)—O(13)	3.42 (2)	K(3)—O(15)	3.88 (2)
K(1)—O(15)	2.99 (2)	K(3)—O(18)	3.05 (2)
K(1)—O(17)	3.33 (2)	K(3)—O(20)	3.34 (2)
K(1)—O(19)	3.73 (2)	K(3) O(22)	3.42 (1)
K(1)—O(20)	3.53 (1)	K(3)—O(24)	3.83 (2)
Mean K(1)—O	3.40 (34)	Mean K(3)—O	3.20 (40)
K(2)—O(1)	3.65 (2)	K(4)—O(2)	3.07 (2)
K(2)—O(4)	2.76 (1)	K(4)—O(4)	3.62 (2)
K(2)—O(5)	3.97 (2)	K(4)—O(6)	3.62 (2)
K(2)—O(7)	3.30 (2)	K(4)—O(9)	3.06 (2)
K(2)—O(9)	3.86 (2)	K(4)—O(10)	2.78 (2)
K(2)—O(11)	3.78 (2)	K(4)—O(11)	2.85 (2)
K(2)—O(16)	3.57 (2)	K(4)—O(12)	3.06 (2)
K(2)—O(18)	3.61 (2)	K(4)—O(13)	3.62 (2)
K(2)—O(21)	2.97 (2)	K(4)—O(16)	3.21 (1)
K(2)—O(22)	3.28 (2)	K(4)—O(19)	3.10 (2)
K(2)—O(23)	3.68 (2)	K(4)—O(21)	3.78 (2)
K(2)—O(24)	2.64 (2)	K(4)—O(23)	3.67 (2)
Mean K(2)—O	3.42 (44)	Mean K(4)—O	3.29 (35)

Table 7. *T*—O—*T* *bond angles* (°) *for hydrothermal* $K_2MgSi_5O_{12}$

Si(2)—O(1)—Si(3)	132 (1)	Si(4)—O(20)—Si(10)	139 (1)
Si(1)—O(2)—Si(4)	152 (1)	Si(2)—O(22)—Si(9)	135 (1)
Si(2)—O(8)—Si(11)	132 (1)	Si(3)—O(23)—Si(7)	157 (1)
Si(3)—O(9)—Si(12)	160 (1)	Mean Si—O—Si	141 (10)
Si(1)—O(11)—Si(8)	134 (1)	Si(4)—O(3)—Mg(6)	136.1 (9)
Si(4)—O(12)—Si(9)	141 (1)	Si(3)—O(4)—Mg(5)	119.8 (8)
Si(8)—O(13)—Si(10)	137 (1)	Si(2)—O(5)—Mg(5)	123.4 (8)
Si(7)—O(14)—Si(11)	145 (1)	Si(1)—O(6)—Mg(6)	133.6 (8)
Si(11)—O(15)—Si(12)	137 (1)	Si(7)—O(7)—Mg(6)	138.7 (9)
Si(8)—O(16)—Si(9)	133 (1)	Si(10)—O(10)—Mg(5)	125.7 (9)
Si(9)—O(17)—Si(10)	130 (1)	Si(8)—O(21)—Mg(6)	147 (1)
Si(7)—O(18)—Si(12)	130 (1)	Si(11)—O(24)—Mg(5)	120.6 (9)
Si(1)—O(19)—Si(12)	160 (1)	Mean Si—O—Mg	130.6 (9.8)

indicated by our results. Thus, it seems likely that the large temperature factor for K in the cubic structure results from a combination of spatial and vibrational disorder. The corresponding temperature factor in the monoclinic structure is much reduced, further indicating the role of spatial disorder in the refinement of this parameter for K.

Framework distortions

We have shown that the tetrahedral-angle variance in dry-synthesized $K_2MgSi_5O_{12}$ leucite is 10.7 deg^2. This value compares with the range 2.1–8.6 deg^2 for the three *T* sites in tetragonal $KAlSi_2O_6$ leucite and a value of 11.9 deg^2 for the single *T* site in pollucite (Beger, 1969). Such distortions in K—Mg leucite are mainly as a result of the disorder of Mg and Si over the single *T* site. The inter-tetrahedral *T*—O—*T* angle is identical to that of pollucite (144.5°; Beger, 1969) and slightly smaller than that of high-temperature natural leucite (145.4°; Peacor, 1968), pointing to similar degrees of framework distortion in all three structures.

The disordered form of $K_2MgSi_5O_{12}$ leucite has a distinctly larger unit-cell volume than the ordered form (2416 and 2348 Å^3, respectively). Thus, the ordering of the Si and Mg tetrahedral cations is accompanied by a contraction of 2.8%, leading to a decrease in the mean *T*—O—*T* angle from 144.5 to 137.4°. This decrease in *T*—O—*T* angle is as a result of the cooperative inter-tetrahedral rotations which occur as a result of Si–Mg ordering and can be considered as reflecting the increased degree of collapse of the framework about the cavity cation (Taylor, 1983). In the ordered structure, the increase in the *T*—O bond lengths from Si—O (1.61 Å) to Mg—O (1.9 Å) is accompanied by a decrease in *T*—O—*T* bond angles from a mean of 141° for Si—O—Si to a mean of 131° for Si—O—Mg; it

seems that the smaller Si—O—Mg angles are directly related to the increased framework collapse in the ordered structure. Indeed, the higher angular variance of the Mg tetrahedra relative to Si tetrahedra (40.4 and 20.9 deg^2, respectively) points to the structural flexibility of the Mg—O tetrahedra in the framework. Equivalent angular-variance values for the Si and Cu tetrahedra in $Cs_2CuSi_5O_{12}$ (Heinrich & Baerlocher, 1991) are 22.7 and 140 deg^2, suggesting that framework structures with Cu tetrahedra will be even more flexible.

Framework ordering and relative stabilities of phases

We have shown that the hydrothermally synthesized $K_2MgSi_5O_{12}$ leucite has a crystal structure derived from that of the dry-synthesized cubic polymorph. Ignoring *T*-site ordering, the two structures are topologically identical. The significant symmetry reduction from the cubic *Ia3d* structure to our refined $P2_1/c$ structure is directly related to the diffusion of Mg and Si on tetrahedral sites within the framework. The ordering of the tetrahedral cations is manifest from the differences in *T*—O bond lengths with Si—O in the range 1.60–1.65 Å, whilst Mg—O bonds are readily distinguished at around 1.9 Å. In contrast, the dry-synthesized sample has no detectable *T*-site ordering, as required by the space group *Ia3d* having a single *T* site.

These results reveal that the structural behaviour of the Mg + Si-substituted leucites studied shows marked differences from that of the leucite-type, $KAlSi_2O_6$. In pure aluminosilicate leucite, the cubic *Ia3d* structure has been assumed to be the stable phase at high temperature, with a displacive transition to a tetragonal ($I4_1/a$), low-temperature structure (*via* an intermediate tetragonal structure, $I4_1/acd$). This transition appears to be driven by the collapse of the aluminosilicate framework around the large cavity site occupied by K, akin to an overdamped soft mode (Palmer, 1990; Boysen, 1990). Hatch, Ghose & Stokes (1990) proposed an alternative mechanism, however, suggesting that the ferroelastic order parameter for the tetragonal–cubic transition was directly related to reversible changes in Al/Si order. In contrast, Palmer & Salje (1990) argued that this displacive phase transition is too rapid to be as a result of Al/Si ordering. Recently, Dove *et al.* (1993) have shown, using static lattice calculations, that Al/Si ordering is unimportant in the cubic–tetragonal transition, and that the observed spontaneous strain does not result from such ordering. The polymorphism revealed in the present study, however, is directly related to such *T*-site ordering occurring during hydrothermal synthesis. It seems that the charge and size of Mg^{2+} (as opposed to Al^{3+}) are sufficiently distinct from those of Si^{4+} to ensure that the fully ordered, thermodynamically more stable monoclinic form is formed relatively rapidly as a result of the catalytic action of water in the hydrothermal synthesis. The mechanisms of formation of the ordered structure are likely to include processes of solution of the disordered glassy starting material followed by recrystallization and subsequent annealing, with protons increasing diffusion and consequent ordering rates (Graham & Elphick, 1991; Goldsmith, 1991). In contrast, the dry-synthesized sample has a 'high-temperature' disordered *T*-site configuration; indeed, the ^{29}Si NMR spectrum for this sample is very similar to that of the glass starting material, reflecting their similar short-range structures (see above; Fig. 1). It seems likely that the absence of catalysing water has led to nucleation and growth rates exceeding rates of diffusion and consequent ordering. The existence of the ordered and disordered forms of $K_2MgSi_5O_{12}$ leucite thus reflects the distinctly different kinetics of the two synthesis techniques employed and, in this case, is not related to a high–low-temperature reversible phase transition. However, the cubic polymorph does represent a stranded metastable state. We expect that the ordered monoclinic structure would approach the cubic, disordered state, possibly through additional intermediate states, on increasing temperature. Whether or not the cubic polymorph exists as a thermodynamically stable phase below the melting point remains the subject of further high-temperature investigations.

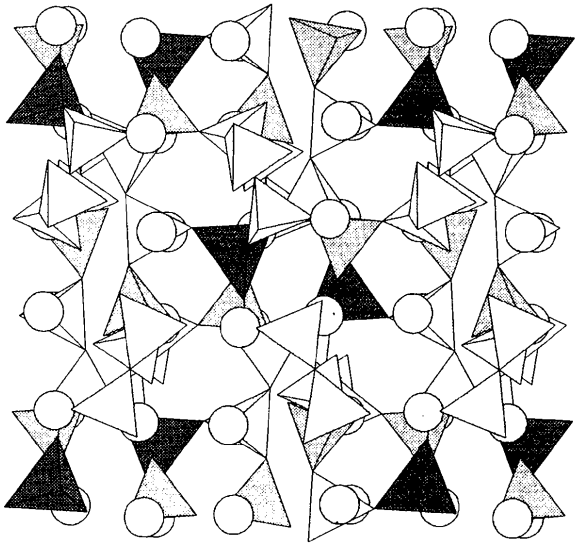

Fig. 7. Monoclinic structure of hydrothermally synthesized $K_2MgSi_5O_{12}$ leucite; projection on (100). Dark shaded tetrahedra represent Mg sites, medium shaded are Q^4(4Si) and light shaded are Q^4(3Si,1Mg) tetrahedra.

The behaviour discussed above is somewhat analogous to that observed in another tetrahedral framework material, cordierite ($Mg_2Al_4Si_5O_{18}$), in which the first material to crystallize from glass is hexagonal but the equilibrium ordered structure (orthorhombic) appears on annealing (Putnis, Salje, Redfern, Fyfe & Strobl, 1987). In both cases there is an increase in *T*-site order together with an accompanying change in crystal system (with an associated ferroelastic strain) as the crystal approaches thermodynamic equilibrium.

Framework connectivity and NMR peak assignments for ordered $K_2MgSi_5O_{12}$

The connectivity information deduced from the NMR spectra (Kohn *et al.*, 1991) and determined in the present work for the ordered sample shows that the Mg tetrahedra are separated by two Si tetrahedra and that the Q^4(4Si) species are also separated by two Q^4(1Mg) Si tetrahedra. In addition, a pair of specific Q^4(1Mg) tetrahedra (*i.e.* same *T*-site number) are separated by two other tetrahedra. Adjacent Mg and Q^4(4Si) tetrahedra are separated by one Si tetrahedron and are located on opposite sides of four rings of tetrahedra (Fig. 7). The energetic disadvantage of Si—O—Mg—O—Mg—O—Si and Si—O—Mg—O—Si—O—Mg—O—Si arrangements within the framework structure is clearly greater than that recognized in aluminosilicates as Al avoidance (Dempsey, Kuhl & Olsen, 1969; Loewenstein, 1954). The monoclinic ordered structure which our refinement has yielded does indeed satisfy this principle as Mg···Mg distances are maximized.

Kohn *et al.* (1991) showed that the two NMR peaks occurring at chemical shifts of −91.0 and −104.5 p.p.m. (relative to tetramethylsilane) resulted from Q^4(4Si) units. They pointed out that the very small shift of −91.0 p.p.m. must correspond to an exceptionally small mean Si—O—Si angle. We can now assign a value of 134.9° to this peak and a Si—O—Si angle of 146.8° for the NMR peak at 104.5 p.p.m. Dupree, Kohn, Henderson & Bell (1992) have used these data to assess the reliability of published correlations between ^{29}Si chemical shifts for Q^4(4Si) units and structural parameters, the principal conclusions being that the linear correlation chemical shift and mean *T*—O—*T* angle cannot be used at small *T*—O—*T* angles, and that when a particular site has a wide distribution of Si—O distances and Si—O—*T* angles, the correlation may break down. In addition, an empirical correlation between chemical shift and mean *T*—O—*T* angles for Q^4(3Si,1Mg) Si atoms was deduced.

Although the synchrotron powder structural data for the ordered $K_2MgSi_5O_{12}$ sample generally confirm the deductions based on NMR studies, some modifications to the adopted NMR model are required. Kohn *et al.* (1991) used COSY and crystal chemical reasoning to adopt their Model *D* which had different types of tetrahedral sites separated by the maximum number of bonds (see above). In Model *D* every tetrahedral site had four different NNN atoms and no combination was repeated (see Kohn *et al.*, 1991; Table 1). We can now see from the X-ray structure that *T* sites (occupied by Si) 3 and 11 are linked to the same set of NNN atoms (Si 2,7,12 and Mg5), while Si sites 4 and 8 are similarly linked (to Si 1,9,10 and Mg6). Re-analysis of the earlier data shows that the X-ray structure gives an even better fit to the ^{29}Si COSY NMR data than the Model *D* topology proposed by Kohn *et al.* (1991). In particular, the apparent correlations between NMR peaks 2 and 10 and peaks 3 and 5, which were previously unexplained, *are* predicted by the new structure. The one-dimensional ^{29}Si NMR spectrum can now be re-assigned as follows (using the *T*-site numbering of the present paper): Si(2) = peak 1; Si(11) = peak 2; Si(8) = peak 3; Si(10) = peak 4; Si(9) = peak 5; Si(4) = peak 6; Si(7) = peak 7; Si(3) = peak 8; Si(1) = peak 9; Si(12) = peak 10.

It is instructive to consider the relationships between the *T*-site connectivities in ordered monoclinic $K_2MgSi_5O_{12}$ leucite and those in tetragonal

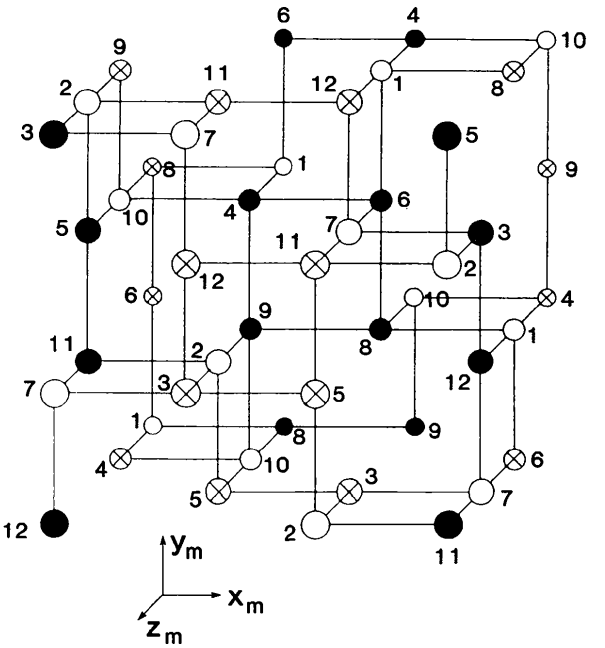

Fig. 8. Schematic idealized unit cell of tetragonal $KAlSi_2O_6$ leucite showing the three different *T* sites (T_1, T_2, T_3; after Murdoch *et al.*, 1988). The numbers refer to the 12 *T* sites determined for monoclinic $K_2MgSi_5O_{12}$ leucite in this work; for an explanation, see text. The axes shown correspond to the coordinate system used by Mazzi *et al.* (1976).

natural leucite (Mazzi *et al.*, 1976). The refined atomic coordinates for both the cubic and monoclinic $K_2MgSi_5O_{12}$ structures reported here are based on a starting model derived from Peacor's (1968) high-temperature cubic leucite ($KAlSi_2O_6$) structure. Comparison of the present data with NMR results and with reported tetragonal structures necessitates a transformation of axes. This is because the NMR *T*-site assignments have been based on tetragonal structures such as that of Mazzi *et al.* (1976). Denoting the crystallographic axes of Mazzi *et al.* as x_m, y_m, z_m, our atomic coordinate system x, y, z is related to the Mazzi *et al.* tetragonal cell by the transformations $x \rightarrow z_m$, $y \rightarrow x_m + \frac{1}{2}$, $z \rightarrow y_m$. Making these transformations, our monoclinic *T*-site assignments can be compared with the various proposed NMR models (*e.g.* Kohn *et al.*, 1991) using the type of stylized structural diagram (Fig. 8) that was first introduced by Murdoch *et al.* (1988) in their discussion of tetragonal $KAlSi_2O_6$. Thus, the monoclinic leucite *T* sites (*T*1–*T*12) can be compared with the three tetragonal *T* sites of $I4_1/a$ leucite (denoted T_1, T_2 and T_3 to avoid confusion). It is clear from Fig. 8 that there is not a simple subgroup–supergroup relationship between the ordering patterns of the $I4_1/a$ and $P2_1/c$ structures. While certain monoclinic sites {*T*1[Q^4(3Si,1Mg)], *T*2[Q^4(3Si,1Mg)], *T*7[Q^4(3Si,1Mg)] and *T*10[Q^4(3Si,1Mg)]} correspond to tetragonal T_2 sites exclusively, the other monoclinic *T* sites {*T*3[Q^4(3Si,1Mg)], *T*4[Q^4(3Si,1Mg)], *T*5(Mg), *T*6(Mg), *T*8[Q^4(3Si,1Mg)], *T*9[Q^4(4Si)], *T*11[Q^4(3Si,1Mg)] and *T*12[Q^4(4Si)]} are all distributed over two tetragonal T_1 and two tetragonal T_3 sites in the unit cell. This reflects the essential difference between tetragonal T_2 and tetragonal T_1 and T_3 sites; the latter each form distinct four-membered rings in the *xy* plane in the unit cell, whereas the former act as inter-ring links (Fig. 8).

Research grants from the NERC (GR3/7496A and GR3/7197) and SR beamtime support from SERC have supported different aspects of this research. We also acknowledge the use of the SERC-funded Chemical Database Service at Daresbury.

References

BEGER, R. M. (1969). *Z. Kristallogr.* **129**, 280–302.

BOYSEN, H. (1990). *Phase Transitions in Ferroelastic and Coelastic Crystals. Cambridge Topics in Mineral Physics and Chemistry*, edited by E. K. H. SALJE, pp. 334–349. Cambridge Univ. Press.

CERNIK, R. J., MURRAY, P. K., PATTISON, P. & FITCH, A. N. (1990). *J. Appl. Cryst.* **23**, 292–296.

DEMPSEY, E., KUHL, G. H. & OLSEN, D. H. (1969). *J. Phys. Chem.* **73**, 387–390.

DOVE, M. T., COOL, T., PALMER, D. C., PUTNIS, A., SALJE, E. K. H. & WINKLER, B. (1993). *Am. Mineral.* **78**, 486–499.

DUPREE, R., KOHN, S. C., HENDERSON, C. M. B. & BELL, A. M. T. (1992). *Calculation of NMR Shielding Constants and Their Use in the Determination of the Geometric and Electronic Structures of Molecules and Solids*, NATO ASI Volume, edited by J. A. TOSSELL, pp. 421–430.

FAUST, G. T. (1963). *Schweiz. Mineral. Petrogr. Mitt.* **43**, 165–195.

GALLI, E., GOTTARDI, G. & MAZZI, F. (1978). *Mineral. Petrogr. Acta*, **22**, 185–193.

GOLDSMITH, J. R. (1991). *Diffusion, Atomic Ordering and Mass Transport*, edited by J. GANGULY, pp. 221–247. New York: Springer-Verlag.

GRAHAM, C. M. & ELPHICK, S. C. (1991). *Diffusion, Atomic Ordering and Mass Transport*, edited by J. GANGULY, pp. 248–285. New York: Springer-Verlag.

HATCH, D. M., GHOSE, S. & STOKES, H. T. (1990). *Phys. Chem. Miner.* **17**, 220–227.

HEINRICH, A. R. & BAERLOCHER, CH. (1991). *Acta Cryst.* C**47**, 237–241.

ITO, Y., KUEHNER, S. & GHOSE, S. (1991). *Z. Kristallogr.* **197**, 75–84.

KIMATA, M. & II, N. (1981). *Neues Jahrb. Mineral. Monatsh.* pp. 1–10.

KLEIN, J. F. C. (1884). *Ges. Wiss. Göttingen Nachr. Jahre*, pp. 421–472.

KOHN, S. C., DUPREE, R., MORTUZA, M. G. & HENDERSON, C. M. B. (1991). *Phys. Chem. Miner.* **18**, 144–152.

LOEWENSTEIN, W. (1954). *Am. Mineral.* **39**, 92–96.

MAZZI, F., GALLI, E. & GOTTARDI, G. (1976). *Am. Mineral.* **61**, 108–115.

MURDOCH, J. B., STEBBINS, J. F., CARMICHAEL, I. S. E. & PINES, A. (1988). *Phys. Chem. Miner.* **15**, 370–382.

MURRAY, A. D., COCKCROFT, J. K. & FITCH, A. N. (1990). *Powder Diffraction Program Library (PDPL)*. Univ. College, London.

PALMER, D. (1990). *Phase Transitions in Ferroelastic and Coelastic Crystals. Cambridge Topics in Mineral Physics and Chemistry*, edited by E. K. H. SALJE, pp. 350–366. Cambridge Univ. Press.

PALMER, D. C., BISMAYER, U. & SALJE, E. (1990). *Phys. Chem. Miner.* **17**, 259–265.

PALMER, D. & SALJE, E. (1990). *Phys. Chem. Miner.* **17**, 444–452.

PEACOR, D. R. (1968). *Z. Kristallogr.* **127**, 213–224.

PUTNIS, A., SALJE, E., REDFERN, S. A. T., FYFE, C. A. & STROBL, H. (1987). *Phys. Chem. Miner.* **14**, 446–454.

RIETVELD, H. M. (1969). *J. Appl. Cryst.* **2**, 65–71.

ROBINSON, K., GIBBS, G. V. & RIBBE, P. H. (1971). *Science*, **172**, 567–570.

TAYLOR, D. (1983). *Mineral. Mag.* **47**, 319–326.

TAYLOR, D. & HENDERSON, C. M. B. (1968). *Am. Miner.* **53**, 1476–1489.

TORRES-MARTINEZ, L. M. & WEST, A. R. (1986). *Z. Kristallogr.* **175**, 1–7.

TORRES-MARTINEZ, L. M. & WEST, A. R. (1989). *Z. Anorg. Allg. Chem.* **573**, 223–230.

WYART, M. J. (1940). *Bull. Soc. Fr. Mineral. Cristallogr.* **63**, 5–17.